Geophys. J. Int. (2009) **177,** 676–690 doi: 10.1111/j.1365-246X.2009.04089.x

Fault-kinematic and geomorphic observations along the North Tehran Thrust and Mosha Fasham Fault, Alborz mountains Iran: implications for fault-system evolution and interaction in a changing tectonic regime

A. Landgraf,[1] P. Ballato,[1] M. R. Strecker,[1] A. Friedrich,[2] S. H. Tabatabaei[3] and M. Shahpasandzadeh[4]

[1] *Institut für Geowissenschaften, Universität Potsdam, Potsdam, Germany. E-mail: landgraf@uni-potsdam.de*
[2] *Department für Geo- und Umweltwissenschaften, Universität München, Germany*
[3] *Building and Housing Research Center, Tehran, Iran*
[4] *Kerman Graduate University of Technology, Kerman* 763113-3131, *Iran*

Accepted 2008 December 19. Received 2008 December 19; in original form 2008 February 26

SUMMARY

Neighbouring faults can interact, potentially link up and grow, and consequently increase the seismic and related natural hazards in their vicinity. Despite evidence of Quaternary faulting, the kinematic relationships between the neighbouring Mosha Fasham Fault (MFF) and the North Tehran Thrust (NTT) and their temporal evolution in the Alborz mountains are not well understood. The ENE-striking NTT is a frontal thrust that delimits the Alborz mountains to the south with a 2000 m topographic front with respect to the proximal Tehran plain. However, no large instrumentally recorded earthquakes have been attributed to that fault. In contrast, the sigmoidally shaped MFF is a major strike-slip fault, located within the Alborz Mountains. Sinistral motion along the eastern part of the MFF is corroborated by microseismicity and fault kinematic analysis, which documents recent transtensional deformation associated with NNE–SSW oriented shortening. To better understand the activity of these faults on different timescales, we combined fault-kinematic analysis and geomorphic observations, to infer the kinematic history of these structures. Our fault kinematic study reveals an early dextral shear for the NTT and the central MFF, responsible for dextral strike-slip and oblique reverse faulting during NW-oriented shortening. This deformation regime was superseded by NE-oriented shortening, associated with sinistral-oblique thrusting along the NTT and the central-western MFF, sinistral strike-slip motion along subsidiary faults in the central MFF segment, and folding and tilting of Eocene to Miocene units in the MFF footwall. Continued thrusting along the NTT took place during the Quaternary. However, folding in the hanging wall and sinistral stream-offsets indicate a left-oblique component and Quaternary strike-slip reactivation of the eastern NTT-segment, close to its termination. This complex history of faulting under different stress directions has resulted in a composite landscape with inherited topographic signatures. Our study shows that the topography of the hanging wall of the NTT reflects a segmentation into sectors with semi-independent uplift histories. Areas of high topographic residuals and apparent high uplift underscore the fault kinematics. Combined, our data suggest an early mechanical linkage of the NTT and MFF fault systems during a former dextral transpressional stage, caused by NW-compression. During NE-oriented shortening, the NTT and MFF were reactivated and incorporated into a nascent transpressional duplex. The youngest manifestation of motion in this system is sinistral transtension. However, this deformation is not observed everywhere and has not yet resulted in topographic inversion.

Key words: Geomorphology; Continental neotectonics; Tectonics and landscape evolution; Asia.

1 INTRODUCTION

Interaction of faults or their segments in tectonically active regions are observed on different temporal scales, ranging from rupture propagation in singular earthquake events (e.g., Stein *et al.* 1997; Hubert-Ferrari *et al.* 2000; Hartleb *et al.* 2002; Wesnousky 2006) over decades to millions of years (e.g. Meyer *et al.* 1998; Peltzer *et al.* 2001; Barka *et al.* 2002; Anderson & Ji 2003; Anderson *et al.* 2003; Armijo *et al.* 2003; Eberhart-Phillips *et al.* 2003; Bennett *et al.* 2004; Lin & Stein 2004; Spotila & Anderson 2004). A better knowledge of temporal aspects of faulting therefore is relevant for the evaluation of seismotectonic segments and associated landscape development that span the Quaternary and beyond.

Fault interaction is also observed at a range of spatial scales involving an alternation of slip rates on neighbouring fault systems (Rockwell *et al.* 2000; Peltzer *et al.* 2001; Pollitz & Sacks 2002; Friedrich *et al.* 2003; Bennett *et al.* 2004; Niemi *et al.* 2004; Dolan *et al.* 2007). Conversely, at the spatial scale of a single mountain front sustained faulting can occur over timescales of 10^4–10^6 yr within discrete seismotectonic segments, apparently without interfering with adjacent segments (Arrowsmith & Strecker 1999; Strecker *et al.* 2003).

The effects of fault propagation also can be studied at various scales and are in the broadest sense compatible with each other, as well as with laboratory studies at various smaller scales or modelled results of joint propagation. The relative motion of the fracture (fault) surfaces (opening, sliding or tearing mode) causes differences in the stress field near the tips, resulting in different styles of propagation (Pollard & Aydin 1988; Pollard & Fletcher 2005). However, the magnitudes of these stress components depend upon the fracture geometry away from the tipline and the loading conditions. Thus, faulting is a process that can involve several different physical mechanisms, which may differ depending upon the rock type and the tectonic setting (Pollard & Fletcher 2005).

These relationships underscore the different levels in the complexity of fault development and the necessity to identify and evaluate spatiotemporal fault behaviour. Faulting scenarios may become even more complex if a re-orientation of the tectonic stress field triggers the reactivation of dip-slip faults as obliquely slipping or pure strike-slip faults (Strecker *et al.* 1990). Alternatively, deformation may be partitioned into a number of different faults, each with different kinematics and pronounced temporal variation (Sanderson & Marchini 1984; Teyssier *et al.* 1995).

Fault linkage and subsequent interaction on the field-scale has been primarily studied in detail in extensional settings (e.g. Dawers *et al.* 1993; Cowie *et al.* 1993, 2000; Armijo *et al.* 1996; Densmore *et al.* 2003, 2007), and from the perspective of strike-slip partitioning and weak versus strong fault behaviour, particularly along the San Andreas Fault (e.g. Zoback *et al.* 1987; Teyssier & Tikoff 1998; King *et al.* 2005), where fault-normal crustal compression parallel to the strike-slip fault is observed. Other natural examples are from segmented strike-slip faults, including geometric observations resulting from spacing or contractional or extensional overlaps (e.g. Bilham & King 1989; Aydin & Schultz 1990; Brankman & Aydin 2004). Fault propagation has been detailed studied in areas of blind thrusts, where it results in the lateral growth of hanging wall anticlines with subsequent imprints in the landscape (e.g. Burbank *et al.* 1996; Jackson *et al.* 1996; Keller *et al.* 1998, 1999; Burbank *et al.* 1999; Jackson *et al.* 2002b). However, on a regional scale, the problem of fault interaction and the effects of a changed tectonic stress field on the kinematic evolution of faults in areas governed by shortening seems less well understood.

The Alborz mountains of Iran are a tectonically active range, where such fault interactions can be studied at the scale of range bounding faults, several tens of kilometres long. Two prominent faults along the southern border of the central Alborz mountains are the North Tehran Thrust (NTT), immediately north of Tehran, and the Mosha Fasham Fault (MFF) to the east (Fig. 2). The kinematic relationship and interaction between these neighbouring faults is an unresolved problem in the late Cenozoic evolution of this mountain range. An improved understanding of the nature of possible interaction between these faults is, however, crucial for the evaluation of regional tectonic activity, and the overall assessment of the evolution of fault systems in the Alborz range, which accommodate almost one third of the intracontinental deformation in Iran. GPS measurements revealed NNE-directed shortening with a rate of 5 ± 2 mm yr^{-1} (Vernant *et al.* 2004a,b). In addition, a range-wide shearing is observed at a rate of 4 ± 2 mm yr^{-1}, which is associated with left-lateral motion on E–W striking structures (Fig. 1). In regions of low deformation rates, morphological indicators in the landscape might suggest important Quaternary tectonic activity along discrete faults, which would correspond to widely distributed deformation in space and time. Along the NTT, the relief increases to more than 3000 m over the Tehran plain, suggesting that the fault has accommodated significant amounts of strain or high strain rates in the Tehran region. The MFF has been inferred to accommodate a significant amount of the observed lateral shearing in the range (Allen *et al.* 2003; Vernant *et al.* 2004a,b; Ashtari *et al.* 2005; Ritz *et al.* 2006). The eastern fault termination of the NTT probably marks the junction with the MFF (Tchalenko 1974; Allen *et al.* 2003). Here, the orientation of the E–W striking NTT agrees with similar striking thrusts and fold axes that are partly cut by the MFF farther east.

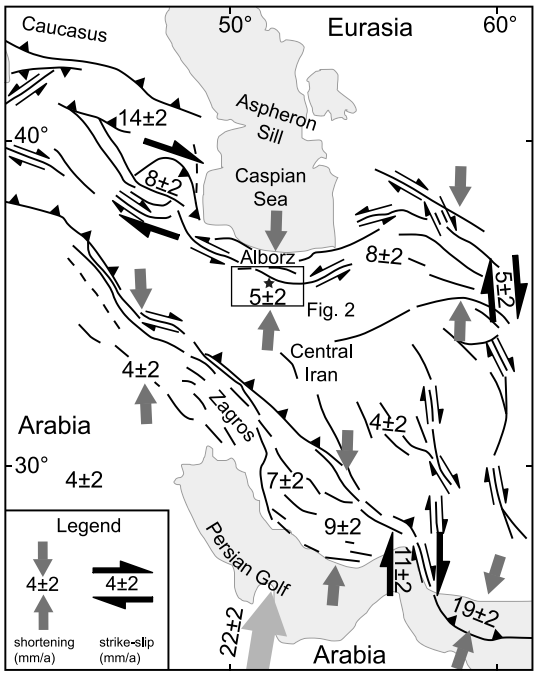

Figure 1. Simplified tectonic map of the Middle East with arrows showing sense of relative motion. Relative displacement in the central Alborz mountains occurs at rates of 5 ± 2 mm a^{-1} and 4 ± 2 mm a^{-1} for shortening and shearing, respectively (modified after Vernant *et al.* 2004a). The box indicates the study area in the south-central Alborz mountains, Fig. 2. Note the approximate location of Tehran (marked as star).

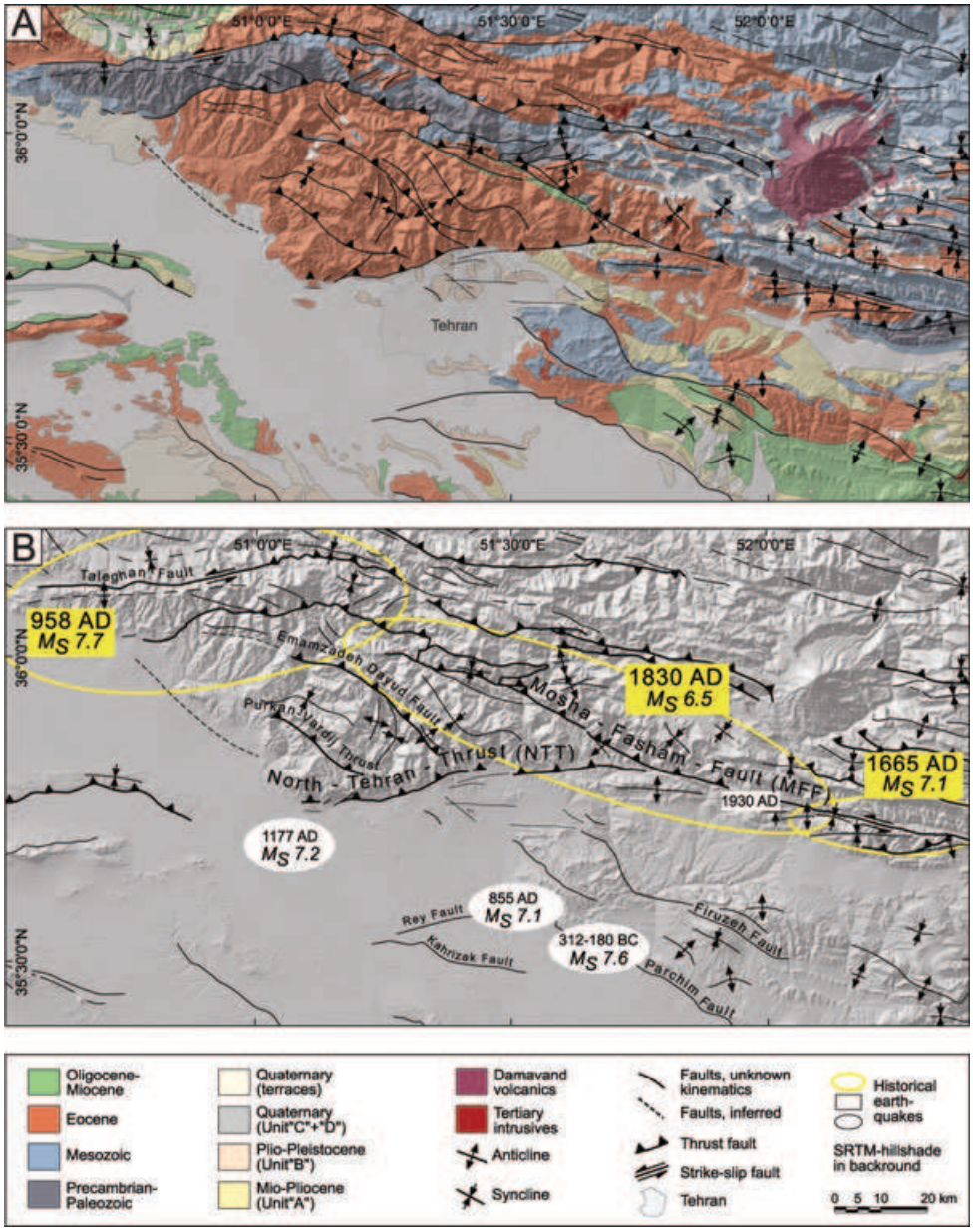

Figure 2. Simplified geology (a) and structural map (b) showing faults of interest and historical earthquakes (modified after Geological Map of Iran, 1:250 000 sheets Tehran, Saveh, Amol and Qazvin-Rasht; historical earthquake data after – rectangles Tchalenko (1974), – white ellipses DeMartini *et al.* (1998) and – yellow ellipses Berberian & Yeats (1999)).

Several historical earthquakes are attributed to ruptures of different segments of the MFF that have affected this fault along its entire length (Tchalenko 1974; Ambraseys & Melville 1982; Berberian 1983; Berberian & Yeats 2001). In contrast, recent seismicity and manifestations of active faulting are limited to the eastern segment of the MFF, indicating sinistral motion. Interestingly, in the vicinity of both faults, instrumentally recorded earthquakes do not exceed magnitudes of 5.5 (Tchalenko 1974). However, historical reports of damage in the vicinity indicate that $M > 7.0$ events may occur on these faults, suggesting that the instrumental record may not yet have recorded the large magnitude events that accommodate much of the relative motions in the area (Tchalenko 1974; Ambraseys & Melville 1982; Berberian 1983; Berberian & Yeats 2001).

It is not known whether or not this gap in seismicity may be associated with a change in the slip rate on adjacent faults, as observed in other tectonically active regions (e.g. Bennett *et al.* 2004). In the Alborz mountains this is a critical aspect, because the NTT apparently merges with the MFF in an area, where the strike of the MFF changes, and where the boundary between recently active and apparently quiescent fault segments occurs.

In this study we characterize the style of deformation observed along the different fault segments of the MFF and NTT. Our field observations constrain the distribution of deformation within the southern Alborz mountains. Fault kinematics, structural data, and geomorphic observations indicate that the deformation field has changed over time. Using these data, we can reconstruct the history of deformation to infer how the development of deformation may be related to a changing stress field in this area. We document the kinematic evolution of the fault system and its link to the landscape development. Based on this information, we present different

fault-kinematic scenarios and test their viability for the transition zone between the MFF and the NTT.

2 METHODS

Fault kinematic measurements were recorded mainly in the hanging wall along the different fault segments. The sense of movement was derived from kinematic indicators, such as Riedel shears or fibrous mineral steps of slickensides. The data were separated into discrete kinematic populations based on overprinting criteria. Concentrations of average *P*- and *T*-axes were determined, and *P*- and *T*-quadrants constructed to yield pseudo-fault plane solutions that are readily comparable with earthquake fault plane solutions (using FaultKin Linked Bingham distribution, Allmendinger 2001).

We used detailed geomorphic observations to assess the landscape response to cumulative displacement and to address the issue of tectonic activity on Quaternary timescales. In addition, the mapping of offset geomorphic markers was supported by analysis of Corona and Aster satellite data, and airphotos at the scale of 1:40 000. Airphotos and 10 m-DEM were made available to us by the National Cartographic Center (NCC), Iran. For limited areas, not fully covered by the NCC-DEM, we have used Shuttle Radar Topography Mission (SRTM) data with 90 m resolution. From these data, we have calculated the topographic residuals, following a flow chart from Hilley *et al.* (1997).

3 GEOLOGICAL AND STRUCTURAL SETTING

The stratigraphic sequence of the southern central Alborz mountains is characterized by an up to 13-km-thick succession of Precambrian to Quaternary strata, deformed and uplifted during two main tectonic events (Assereto 1966). A Cambrian to middle Triassic platform sequence is interpreted to correspond to the northern rim of Gondwana (Kürsten 1980). The oldest contractional event, the Cimmerian orogeny, started in late Triassic after collision of the Iranian microplate with Eurasia and resulted in emerged areas and a regional unconformity, covered by the Shemshak Formation (Assereto 1966; Kürsten 1980; Davoudzadeh & Schmidt 1984; Alavi 1991, 1996; Stampfli & Borel 2002). In the central Alborz however, the Cimmerian orogeny was associated with the late-stage formation of grabens (Zanchi *et al.* 2006). Cretaceous carbonate and volcanic rocks were deformed during contractional reactivation of these extensional structures. Palaeocene conglomerates and limestones cover the folded strata (Assereto 1966). A sequence of up to 5-km-thick Eocene volcanic rocks, volcanoclastic sediments, and shale (Karaj Formation) overly the deformed Cretaceous rocks and appear to have formed in an extensional back-arc setting (Guest *et al.* 2006b). Subsequent Oligocene to Miocene shortening caused progressive uplift, and was accompanied by concomitant erosion and sedimentation of fine-grained sandstones and marls (Red Formation). These processes are linked to the onset of the Arabia–Eurasia collision and started about 12 Ma, inferred from accelerated exhumation rates in the Alborz range (Guest *et al.* 2006b).

The southern central foreland basin of the mountain belt comprises extensive alternating conglomerates, silt, and sandstone units (Hezardarreh Formation or Unit A). Based on sedimentary facies correlations with the foreland deposits of the Zagros mountains (Bakhtiari Formation) the inferred age is Late Mio-Pleistocene (Rieben 1955). However, this might represent a simplification, since the Bakhtiari Formation represents diachronus deposits advancing towards the foreland rather than being a uniformly deposited sheet (Fakhari *et al.* 2008). This could also be the case for the Alborz mountains, where a recent study suggested a late Miocene age (7.5–6.2 Ma) for the Hezardarreh Formation exposed along the southern Alborz mountains (Ballato *et al.* 2008). This Formation is in turn unconformably overlain by the Kahrizak Formation (Unit B), which comprises sand- and siltstones, and the Tehran Alluvium (Unit C), a laterized conglomerate (Rieben 1955).

Based on thermochronologic data (Axen *et al.* 2001) and field observations, Allen *et al.* (2003) suggested a two-stage Neogene evolution of the Alborz mountains with (1) Miocene N–S directed shortening, accompanied by limited conjugate right- (western part) and left-lateral (eastern part) strike-slip faulting, and (2) Pliocene-Quaternary NE–SW directed shortening, accompanied by left-lateral strike-slip faulting along the entire length of the mountain range.

Interpretations of the geometry and kinematics of faulting in the Alborz mountains remain controversial (Priestley *et al.* 1994; Jackson *et al.* 2002a; Allen *et al.* 2003; Guest *et al.* 2006a). There appears to be general consensus about sinistral transpression with strain partitioning involving dip-slip shortening and strike-slip faulting. More than 30 per cent of the shortening is associated with seismic activity, whose sense of motion indicates that shortening is partitioned into left-lateral strike slip and thrusting in the WNW-trending high Alborz range and reverse faulting with a left-lateral oblique component of motion at lower sectors (Priestley *et al.* 1994). In contrast, coeval with the transpressional deformation, the internal domain of the central Alborz mountains is characterized by recent transtension (Ritz *et al.* 2006). Here, the geomorphic characteristics of the landscape traversed by the neighbouring Taleghan, eastern Mosha Fasham and Firuzkuh faults documents left-lateral kinematics with a minor normal component. This kinematic system is compatible with a general strike-slip regime and a local change in the position of σ_1 from a regional horizontal position (Shmax) to a vertical one between the borders and the internal domain (Ritz *et al.* 2006).

3.1 Mosha Fasham Fault

The sigmoidal trace of the MFF is >175 km long and strikes E–W to WNW–ESE, with variable N-dips between 35° and 70° (Tchalenko 1974; Allen *et al.* 2003). Its central part is characterized by a double-bend towards a northwest strike (Fig. 2), which accounts for approximately one third of the entire fault length. The MFF comprises three segments, a western (approximately west of 51°20′E), an eastern (east of 52°E), and the central segment, located between them (Tchalenko 1974; Berberian & Yeats 1999). Importantly, the eastern tip of the MFF is close to the western termination of the active left-lateral (transtensional) Firuzkuh Fault (Allen *et al.* 2003; Ritz *et al.* 2006), whereas the western tip is masked by Quaternary sediments. However, the entire western segment of the MFF strikes parallel to the active, left-transtensional Taleghan Fault (Ritz *et al.* 2006) (compare Fig. 2b).

Deflected streams, offset channels, and fault planes with horizontal striations in the eastern and central-eastern fault sectors indicate left-lateral motion (Allen *et al.* 2003; Ashtari *et al.* 2005; Ritz *et al.* 2006). In addition, thrust and reverse faults are observed, and juxtapose Cambrian with Eocene or Miocene strata. Early shortening at the MFF has been estimated to be on the order of 4 km (Allenbach 1966; Steiger 1966). Fault-plane striations, analysed by Bachmanov *et al.* (2004), reveal faulting with dominant strike-slip in the eastern

part and an equal degree of reverse and strike-slip motion in the central part. Despite these observations, several E-trending folds, aligned along and cut by the MFF, indicate that a former dextral transpressional regime was superseded by sinistral strike-slip faulting. These observations emphasize the significance of the MFF as a long-lived structure which has accommodated shortening under changing stress regimes in the course of the convergence between Eurasia and Arabia.

Allen *et al.* (2003) calculated a maximum sinistral offset of ~35 km, based on piercing points in lower Palaeozoic strata in the eastern and central-eastern segments, which would, assuming the beginning of left-lateral motion 5 Ma ago, correspond to a slip-rate of up to 7 mm a^{-1}. However, Ritz *et al.* (2006) calculate a sinistral slip rate of about 2 mm a^{-1} with a minor normal component. This transtension is in agreement with microseismicity recorded along the eastern MFF, showing left-lateral strike-slip faulting associated with a normal components (Ashtari *et al.* 2005; Ritz *et al.* 2006).

Limited data exist along the western segment, but kinematic indicators show reverse dip-slip to sinistrally oblique reverse faulting near the western terminus, and sinistral oblique-reverse motion near the eastern segment boundary (Guest *et al.* 2006a). In addition, Guest *et al.* (2006a) found minor synthetic faults with a reverse-dextral oblique sense of slip in the hanging wall of the MFF. However, based on syn-kinematic folding, foliations, and s-c fabrics, Moinabadi & Yassaghi (2007) infer a dominance of dip-slip faulting along the western segment.

Several destructive earthquakes occurred in the study area (Fig. 2b), attributed to slip along different segments of the MFF, and possibly motion on blind faults in the foreland (Ambraseys 1974; Tchalenko 1974; Ambraseys & Melville 1982; Berberian 1983; DeMartini *et al.* 1998; Berberian & Yeats 1999, 2001). The three largest damaging earthquakes along the MFF occurred 958, 1665, 1830 and 1930 AD. Damage of the 958 Taleghan-Ray earthquake is reported from an area of more than 200 km in diameter (Ambraseys & Melville 1982). As the Taleghan and western Mosha faults are parallel structures, activity along the Taleghan Fault during the 958 AD earthquake may have been possible.

3.2 North Tehran Thrust

Here, we refer to the NTT as the boundary fault between Karaj in the west and Niknam Deh in the east, where the Eocene rocks of the Alborz range are thrust over Neogene and Quaternary sediments of the Tehran embayment (Tchalenko 1974, 1975; Berberian 1983; Allen *et al.* 2003) (Fig. 2, for locations compare 3a).

The NTT is more than 60 km long, strikes E–W to ENE–WSW and is an oblique thrust or reverse fault with a left-lateral component of motion (Alavi 1996). North of Tehran NW-striking folds and faults deflect older, N to NE-striking structures, inferred to result from earlier right-lateral motion along the NTT (Allen *et al.* 2003). The NTT fault zone comprises numerous subparallel, right-stepping en échelon segments, as well as NW-striking thrusts, the Purkan-Vardij Thrust (PVT) and the likewise striking Emamzadeh-Davud Fault (EDF) that merge with this fault (Tchalenko 1974; Berberian & Yeats 1999; Allen *et al.* 2003) (Fig. 2b).

The western segment (west of 51°15′E) comprises a ramp-flat geometry, following the limbs of a footwall anticline at the right-hand bank of the river Kan (for location compare Fig. 3a). Two kilometres west of this location the fault trace becomes discontinuous. It is much more subtle and locally associated with NE- or E-striking thrusts (Tchalenko 1974). Locally, vertically dipping

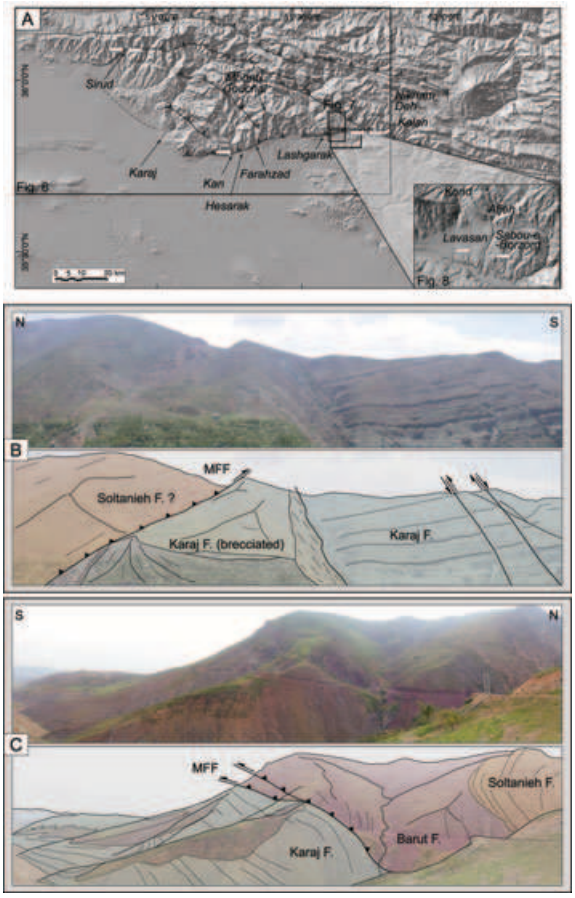

Figure 3. Overview map and field examples of folding and faulting associated with the western MFF fault segment. (a) Regional overview map showing main faults and location names as mentioned in the text. Boxes indicate following figures (inset is zoom of Fig. 8 box), while white arrows show locations of field photos (panels b and c and Fig. 4) and point in view direction. (b) View towards E showing the MFF at Sirud (western segment). Here, the fault has thrust characteristics with Cambrian units juxtaposed against Eocene Karaj Formation. (c) View towards W showing the MFF between Sirud and Velijan (western segment). The overall impression of the fault geometry suggests thrusting, while fault-kinematic measurements indicate sinistral reactivation (compare Fig. 5b, 23). Note the footwall syncline in the Karaj Formation (middle ridge), compatible with primary thrust kinematics.

Plio-Pleistocene sediments abut in fault contact horizontal to gently dipping Eocene tuffs.

The central-western segment, between 51°15′ and 51°28′E, is characterized by thrusting and reverse faulting at an increasingly steeper fault plane towards east. This segment is itself subdivided into several en échelon faults (Tchalenko 1974).

The central-eastern segment, between 51°28′ and 51°34′E, however, is characterized by a broad zone of thrusting (Tchalenko 1974). East of Lashgarak (for location compare Fig. 3a), the fault termination probably marks the junction with the MFF (Tchalenko 1974; Allen *et al.* 2003; Bachmanov *et al.* 2004). This region is intensely folded, although the topography is much more subdued compared to that of surrounding regions. Here, the NTT strikes E–W, parallel to other thrusts and fold axes that merge with the MFF or are cut by it (Fig. 2).

Faulting and folding of the piedmont south of the NTT suggests a shift of the deformation into the foreland. Deformation of

the piedmont consists of four subparallel E–W oriented anticlines, involving the 'A' Formation, which is unconformably overlain by almost horizontally bedded 'B' Formation deposits (Engalenc 1968). The folds are asymmetric, with steep northern limbs, which are partly overturned and developed into S-verging flexures and reverse faults (Tchalenko 1974). In addition to these thrusts, NW-striking faults are observed in the central and western piedmont (Tchalenko 1974).

4 FAULT KINEMATIC DATA

Different structural trends along the southern Alborz range can be identified that allow us to develop a relative faulting chronology, based on cross-cutting relationships, and the relative age of the involved units. In this section, we first discuss the macroscopic structures and subsequently present fault-slip data collected on major and minor faults. Combined, these data help unravel the kinematic history of the southern Alborz range.

In the NTT hanging wall, subparallel to obliquely oriented (Niknam Deh, west; Fig. 4a) fold axes are exposed. At the western and the eastern (Niknam Deh, east; Fig. 4b) tips of the NTT, NE-striking meso- to macroscale folds affect the Eocene Karaj Formation. In one case the folds are unconformably overlain by tilted, SE-ward dipping Plio-Pleistocene Unit A deposits.

ENE- to ESE-striking faulting with dominant dip-slip movement and occasional dextral and sinistral components is observed at the western segment of the MFF (Figs 3b and c), but also affects the Karaj Formation and is linked with activity on the NTT (Figs 5a, 2 and 4). In addition, NW- to N-striking faults with medium to high-angle dips were observed along the entire length of the NTT, generally affecting the Karaj- and Miocene Red formations. In the western area, the offset pattern along these faults is consistent with either west-side down displacement or left-lateral motion (Fig. 5a, 1 and 3). Close to the eastern termination of the NTT, these faults are exposed in the NTT hanging wall and the MFF footwall, either displaying motion partitioned into strike-slip and dip-slip components or oblique kinematics resulting in associated flower structures.

In the eastern part of the study area approximately E-striking high-angle faults were observed that we term the Latyan fault zone. These faults affect mainly Unit A deposits (but more recent sediments cannot be excluded). Faulting has resulted in a cataclastic zone, to 1–2 m wide, with rotated clasts obliquely oriented and forming large shear bands. The tectonized clasts and an offset palaeosoil (Figs 4g, e and f, respectively) show a vertical sense of movement, although limited subhorizontal fault striations may indicate a strike-slip reactivation of this structure. In some cases these faults have flower-structure geometries, indicating oblique motion. The same set of faults also occurs occasionally in the Miocene Red Formation farther east where it is associated with motion along the MFF.

The youngest tectonic manifestations are N-striking thrust faults cutting alluvial deposits (from Unit A to Unit C) away from the range in the Tehran plain. These thrusts have been observed only in the western and central parts of the NTT footwall and either verge west- or eastward.

Our data and observations by other workers show that these structures are not compatible with one sustained kinematic regime. Instead, the kinematic analysis and our synthesis of macrostructures reveal two separate kinematic regimes that have influenced the NTT and MFF (Figs 5a and b). We infer that these regimes were controlled by a rotation of the shortening direction from an original NW–NNW to a neotectonic NE–NNE orientation. This may have resulted from a rotation of the direction of the greatest horizontal stress S_{Hmax}. These interpretations are based on Anderson's theory of faulting (Anderson 1905, 1951), whereupon faults form at specific angles to the applied principle stresses and where one stress direction is vertical. However, this theory relates the orientation of faults to the stress field at the time of development. Once formed, the faults remain zones of weakness, which might be reactivated, even if the regional stress field is not optimally oriented. In this case, the state of stress does not control the orientation of the fault plane, but instead controls the slip vector, whose orientation depends on the stress tensor aspect ratio (e.g. Célérier 1995). In addition to these complexities, we have to consider that even in small regions, the stress field may vary and become inhomogeneous. However, in our study area, faulting in both regimes has been accompanied by macroscale and mesoscale folding (compare insets in Figs 5a and b, respectively), which we think is another indicator for the rotation of the shortening direction and supports the applicability of Anderson's theory.

It is interesting, however that indicators of sinistral motion along the central segment of the MFF are rare. Such kinematics are instead often associated with E-striking subsidiary faults (e.g. Fig. 5b, 17 and 14), partly with normal components and the likewise E-striking western MFF segment. These observations imply a strong influence of the fault geometries with respect to the accommodation of regional stresses resulting from the convergence between Arabia and Eurasia.

The earlier NW-oriented shortening episode is compatible with thrusting and dextral strike-slip kinematics on the MFF and NTT (Fig. 5a). The Miocene marls of the Red Formation are the youngest units affected by this kinematic regime. Part of this deformation regime are conjugate low-angle NE- and WNW-striking dextral oblique thrusts, NE-striking thrusts, high-angle NW-striking left-lateral strike-slip faults, NNE-striking reverse faults, and NE-trending folds. This structural inventory is consistent with the macroscale dextral transpressional character of the MFF, as expressed by the alignment of ENE-striking thrusts and folds that are cut by the fault.

NE-shortening is associated with oblique thrusting along the central MFF and in its footwall, as well as sinistral strike-slip faulting on minor faults in the central MFF segment (Fig. 5b). NW-striking reverse and thrust faults, and NNE-striking dextral strike-slip faults constitute the main inventory of the analysed structures. In addition, WNW-trending folds, oblique to the strike of the NTT, are indicative of left-oblique reactivation of the NTT. NW-trending fold axes and macroscale tilting are also observed and attest to the regional accomodation of NE-directed shortening.

In addition to the orientations of the inferred compressive stresses our fault-kinematic data reveal limited examples of extensional pseudo-fault plane solutions (Fig. 5c) with varying orientations of the tension axes. The data were recorded along the MFF and a subsidiary fault-branch as well as along the NTT in the junction area between both faults. In some cases, a combined data analysis, without extraction of the normal components reveals pseudo-fault plane solutions with left-oblique kinematics on W- to NW striking nodal planes (Figs 5c, 7, 14, 16 and 17).

The fault-kinematic analysis of the strained clasts and faults measured in the junction area show recent left-lateral strike-slip and normal faulting [Figs 5b and c (a to h)]. Since these data correspond to the youngest activity, they are in agreement with the geomorphic observations of a kinematic changeover from dip slip to systematically oblique faulting. This is also observed in Oligo-Miocene bedrock units, where the oldest, dextral-transpressional trend is

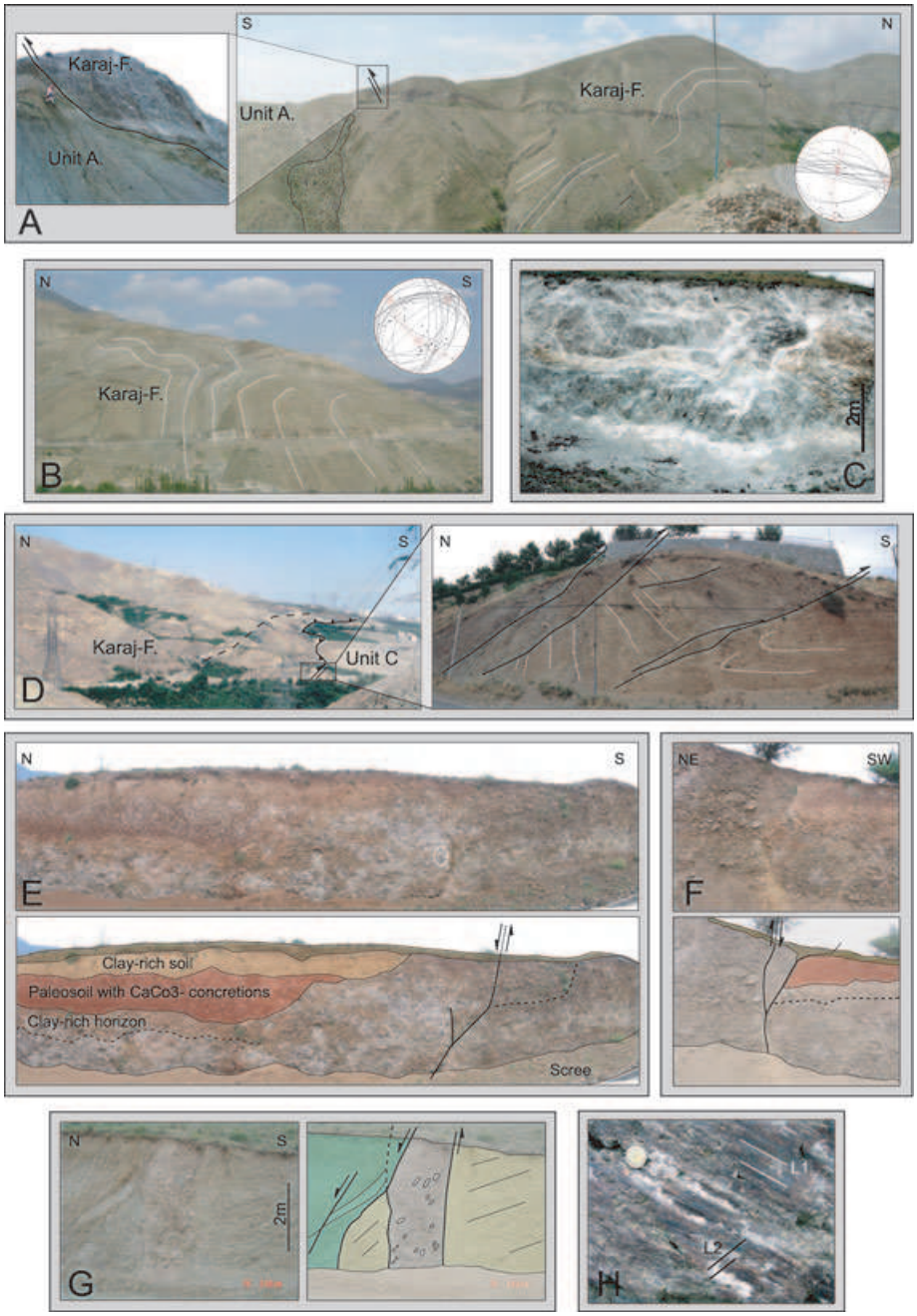

Figure 4. Field examples of folding and faulting associated with the NTT and MFF fault system. (a) NTT exposure west of Niknam Deh (compare arrows at Niknam Deh in Fig. 3(a) for location). The fault trace shows a ramp-flat geometry and the hanging wall exhibits an alternation of synclines and anticlines with axes oblique to the NTT, but compatible with the present-day shortening direction. See inset stereoplot with the calculation of the foldaxis from measurements of the fold limbs. White lines denote bedding in Karaj Formation rocks. Extensive slope debris below the fault trace indicate a cataclastic fault zone. Fault kinematic measurements in tectonized quaternary river gravels show sinistral reactivation (compare Figs 5b (f)) (b) Folding in the hanging wall of the NTT at Niknam Deh, just east of (a), white lines denote bedding, inset stereoplot for axis calculation; note that here the foldaxis is not compatible with the present-day shortening direction. (c) Cataclastic shear zone in volcanic rocks of the Karaj Formation associated with the NTT near Farahzad. No sense of motion or timing of fault activity can be inferred. (d) NTT fault trace (black line with teeth) and possible subsidiary fault (dashed) at Kan (compare arrows at Kan in Fig. 3a for location). This outcrop was previously studied by Tchalenko (1974, 1975) and shows thrusting of cataclastic Karaj Formation rocks over alluvial sediments (possibly Unit B) as well as internal deformation of alluvial units. (e) and (f) High-angle faulting in alluvial deposits at a roadcut in Lavasan (see arrow in inset in Fig. 3a), both outcrops are just some metres apart. The colour coding of the soils is the same. Geological hammer for scale in white circle on (e), note the palaeosoils as marker horizons for faulting. A flower structure geometry of the fault (here informal called Latyan fault) is inferred. The erosional terrace level corresponds to T4 in Fig. 8 and seems to postdate the faulting. (g) High angle, E-striking Latyan fault about 3 km east of (e) and (f) near Sabou-e-Bozorg (see arrow in inset in Fig. 3a). Erosional terrace level corresponds to T2 in Fig. 8. Rotated clasts indicate coarse shear bands in the fault zone, coherent with the drag of the bedding. However, horizontal striations in the fault gouge indicate strike-slip reactivation. (h) Example of reactivation of the MFF with two generations of oblique kinematic indicators; the older Lineation (L1) is associated with slickensides and a polished surface, while superimposed are striated calcite fibres (L2).

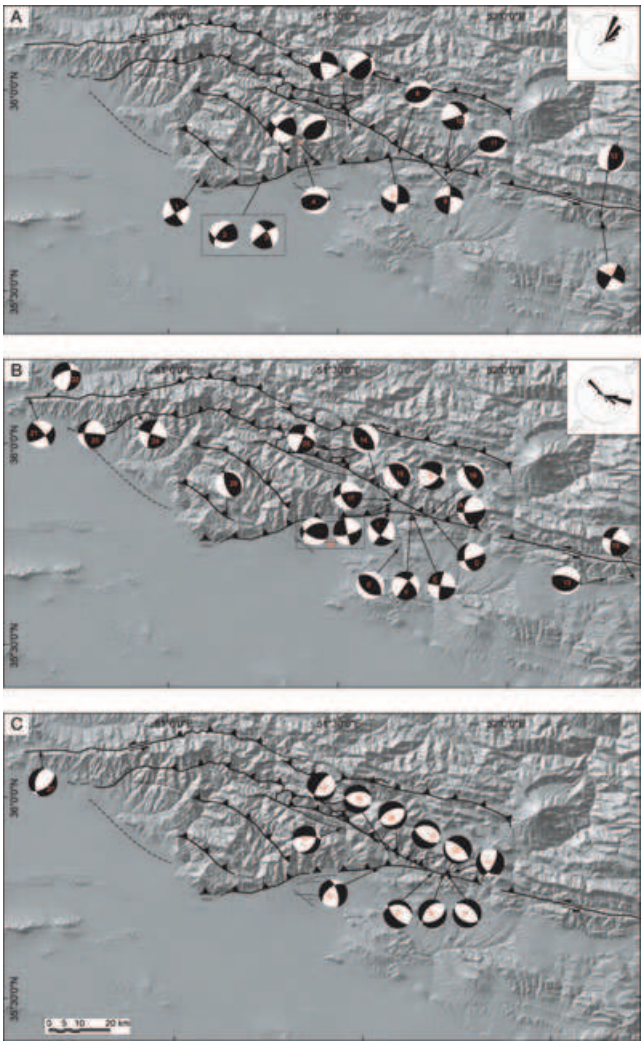

Figure 5. Pseudo-fault plane solutions of measured and sorted fault kinematic data, grouped according to their kinematic populations. The fault kinematic analysis reveals two faulting regimes for the NTT and MFF, controlled by a rotation of S_{Hmax} from an original NW/NNW (a) direction to a NE/NNE orientation (b), note the inset scatter plots of calculated σ_1 poles and the rose diagrams of the measured mesoscale and calculated macroscale foldaxes orientations. In addition, indications of extension were observed, without clear cross-cutting realtionships for the measurements in bedrock (7, 14, 16), but demonstrating the youngest tectonic movement in the quaternary outcrops (c). Fault kinematic raw data (strike, dip, rake and sense of movement) were analysed using the Fault Kin program (Allmendinger 2001) and are downloadable from the data repository.

superseded by a left-transtensional regime. However, the Quaternary faulting history is also very complex and reveals different extension directions. Good conditions for kinematic analysis and trench logging are found in the Kond and Afjeh valleys, and in Kalan. These outcrops show evidence for repeated abrupt offsets, as documented by the sedimentary wedges in the footwall and fissure fills along the fault, and clearly document Quaternary seismogenic activity.

5 GEOMORPHIC OBSERVATIONS

To characterize the distribution of relief in the vicinity of the faults as a proxy for deformation and uplift and to identify areas of young tectonism, we used morphometric and landform analysis of the investigated area.

Morphometric analysis

Localized surface uplift or base-level lowering results in increased channel slopes with higher erosion rates, and therefore increased relief of drainage basins relative to surrounding crests (Merrits and Vincent 1989; Bürgmann *et al.* 1994). Residual relief maps, calculated as the difference between an envelope of the highest elevations and another envelope of the present-day drainage channels, therefore help outline sectors of high stream-incision rates, presumably associated with high rock uplift (Bürgmann *et al.* 1994; Hilley *et al.* 1997). However, the interplay between uplift and erosion is also influenced by differences in erodibilty of the material, e.g. rock type variations in the range, which might account for considerable differences in relief. The following calculations are based on the assumption of spatially uniform resistance of rock to erosion, but are less reliable where this condition is not satisfied. The rock type variability in the Eocene units of the study area is generally high, nevertheless, we think that differences in erodibility of these units are less significant, especially on the scale used for the morphometry. To be more precise, it is worth comparing the area between the NW-prolongation of the NTT and the EDF (compare Fig. 2), where a more than 5 km thick succession of these highly variable Eocene units is exposed. At this location the Karaj-Formation comprises three different shale members, repeatedly alternating with tuffs, tuffaceous siltstones, limestones and sandstones in places, but it does not exhibit any significant difference in residual relief. However, where such rock type variations are obvious and might correspond to the observed relief, we will indicate this possibility in the text.

The residual relief map of the NTT/MFF area exhibits two distinct spots and one elongated zone of high-uplift (Fig. 6b, dark blue areas). The elongated area is located between and aligned with the subvertical western segments of the Mosha Fasham and Taleghan faults. This high is associated with outcrops of Precambrian to Palaeozoic units, which comprise mainly dolomite, sandstone and limestone, and might be more resistant to erosion than the Mesozoic limestone and shales or the Eocene limestones, shales and volcanoclastic sediments. The remaining two zones of high topographic relief do not strikingly correspond to such strong resistant rock types. One of these spots is located immediately east of the outside corner of the MFF left bend, and accordingly, the inside-corner of Taleghan-Fault left bend. However, the third high-relief zone is located around Mount Touchal, at the inside corner of the NTT and EDF (compare Fig. 2a for geology and b for fault names). Here, in the immediate hanging wall of the EDF, the base of the Eocene units is exposed, which also comprise other lithologies, such as lava flows. These units are potentially more resistant. However, the top units of the Touchal, which correspond to the location of the high residual relief, consist of an alternation of shale and tuffaceous siltstone, and are consequently more erodible.

To infer a relation of the relief in the NTT-hanging wall with the relief across the connecting faults (MFF, EDF, PVT-compare Fig. 2b for fault names), a topographic swath profile was calculated, approximately perpendicular to the NW-striking faults (Fig. 6c). In addition to a general eastward increase in topography, the maximum elevation (upper line) has consistently the highest points in the hanging wall of the NW-striking faults. Interestingly, the mean elevation (middle line) drops in the MFF fault zone.

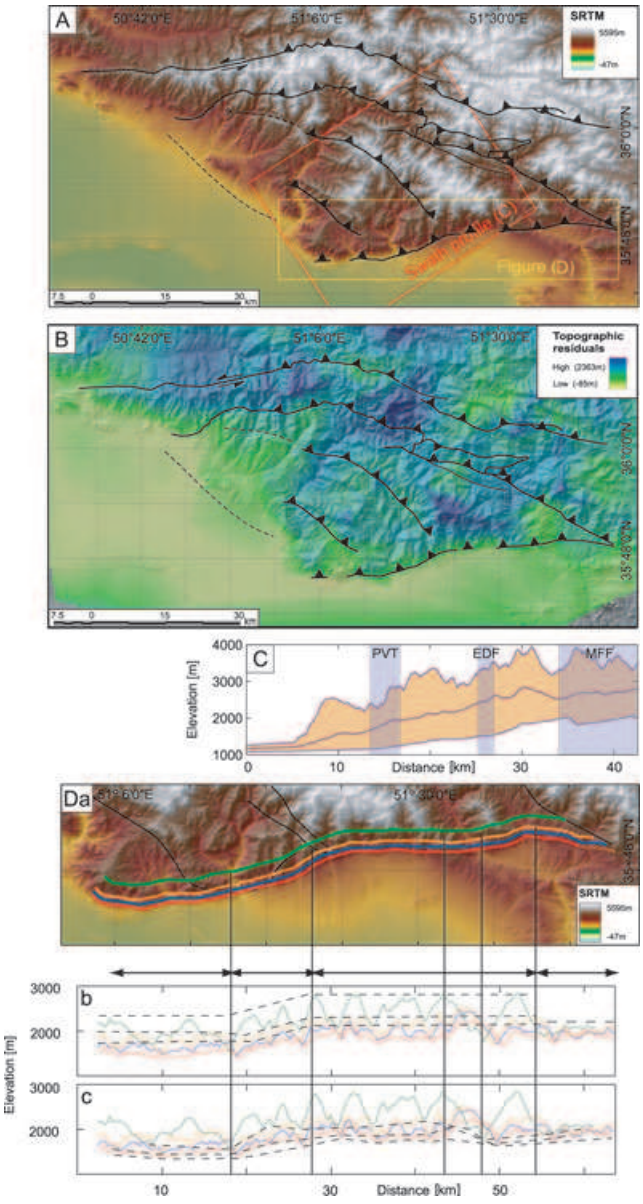

Figure 6. Topographic analysis, derived from DEM data. (A) Overview-DEM with main faults (for labels compare Fig. 2b). Indicated are locations of following figures. (B) Topographic residuals of the study area, derived from SRTM-data by subtracting a drainage-envelope from a ridge-crest envelope. The blue spots correspond to high incision and presumably, high-uplift zones. (C) Topographic swath profile across the NTT and perpendicular to its connecting faults (MFF, EDF, PVT-compare Fig. 2b for fault names) showing the distribution of minimum, maximum and mean elevation. Note that the highest maximum elevation is always located in the hanging wall of these faults. (D) Topographic along-strike profiles in different intervals to the NTT-fault trace. (a) Location of the profiles on SRTM-DEM, colour coding is equivalent to the profile lines in (b) and (c). Note also the locations of the connecting faults (MFF, EDF and PVT) (b) profiles with manual interpolation along the highest peaks; (c) profiles with manual interpolation along the base level. Note the consistent segmentation in (b) and (c) as indicated by the black vertical lines.

For about two thirds of its length, the NTT fault trace constitutes the southern edge of the Alborz mountains. Towards the east, increasing footwall uplift alters this expression. Assuming that topographic relief correlates with cumulative offset (King *et al.* 1988; Stein *et al.* 1988; Bilham & King 1989; Taboada *et al.* 1993), topographic along-strike profiles were calculated in different intervals from the fault trace to characterize the long-term behaviour of the NTT (Fig. 6d). All profiles show consistently two main steps in topography, linked by a transition zone. Thus, the western segment has accumulated less displacement than the central segment. Interestingly, a topographic outlier in the central NTT-segment, which exhibits anomalously high topography, coincides with the termination of a prominent WNW-trending anticline [Latyan structure after Dellenbach (1964)], but is also associated with a subtle right-bend of the NTT (Fig. 6d). This suggests interaction with the NW-ward growing anticline and related faults, which would plunge below the NTT. Towards the east, in the junction area, the topography is much more subdued without any significant differences among the four profiles. This might suggest less accumulated uplift, which could result from a kinematic changeover to dominant strike-slip motion. However, while this kind of analysis requires uniform resistance of rocks to erosion, we cannot exclude that in this easternmost segment, the effect is due to higher erodibility of the exposed shales. Overall, the segmentation of the NTT, as amplified in its distinguishable topographic expression, suggests semi-independent uplift histories.

Interestingly, the position of the Kan river also marks the position of the segment boundary between the western and central segments. Decreasing offsets towards the tips of the overlapping segments might have enhanced the ability of the river to cut through the more slowly rising mountain front. In contrast, catchments in the hanging wall of the rapidly rising central segment are rather steep and small. However, another possibility might be that an early Kan river was able to capture areas in the headwater, which allowed it to continue incising contemporaneous to uplift. In this case, the relief would rather reflect the drainage history than spatial gradients in rock uplift. At present, this cannot be excluded.

Faulting and landform evolution in the NTT/MFF transition area

Where the eastern branch of the NTT approaches the MFF, both faults show a change in strike direction. The MFF changes strike from WNW to NW, while the NTT has a subtle left-hand bend. No small-scale offsets as indicators of motion during the most recent earthquakes were observed along the fault traces, but cumulative offsets reveal the long-term tectonic activity of both faults. For example, three sets of areally extensive Quaternary terraces occur in the footwall of the MFF and in the hanging wall of the NTT, which have no match beyond the fault (Fig. 7).

This clearly documents Quaternary thrusting along the NTT. The geomorphic surface T2, a gravel covered erosion surface, is sculpted into the folded Eocene to Miocene units that have deformed during NE-directed shortening (Fig. 7b). A reconstruction of T2 surface remnants (Fig. 7c) reveals vertical displacement of 317 m relative to the local base level at the NTT. Assuming a Quaternary age of the surface, the offset implies a minimum slip rate of 0.2 mm yr^{-1}. However, this rate could be several mm yr^{-1}, if the surface is only few hundred thousand years old.

Terraces in the hanging wall of the MFF are rare, but the fault trace is characterized by a pronounced step in topography. Channels crossing this structure are not deflected laterally, but recent faulting is manifested by a scarp of a young dip-slip splay fault of the MFF (Fig. 7a).

Distinct sinistral stream offsets of about 85 m characterize the eastern termination of the NTT, east of the area of thrusting (Fig. 8a). In addition, the deformation history of the NTT-footwall reveals

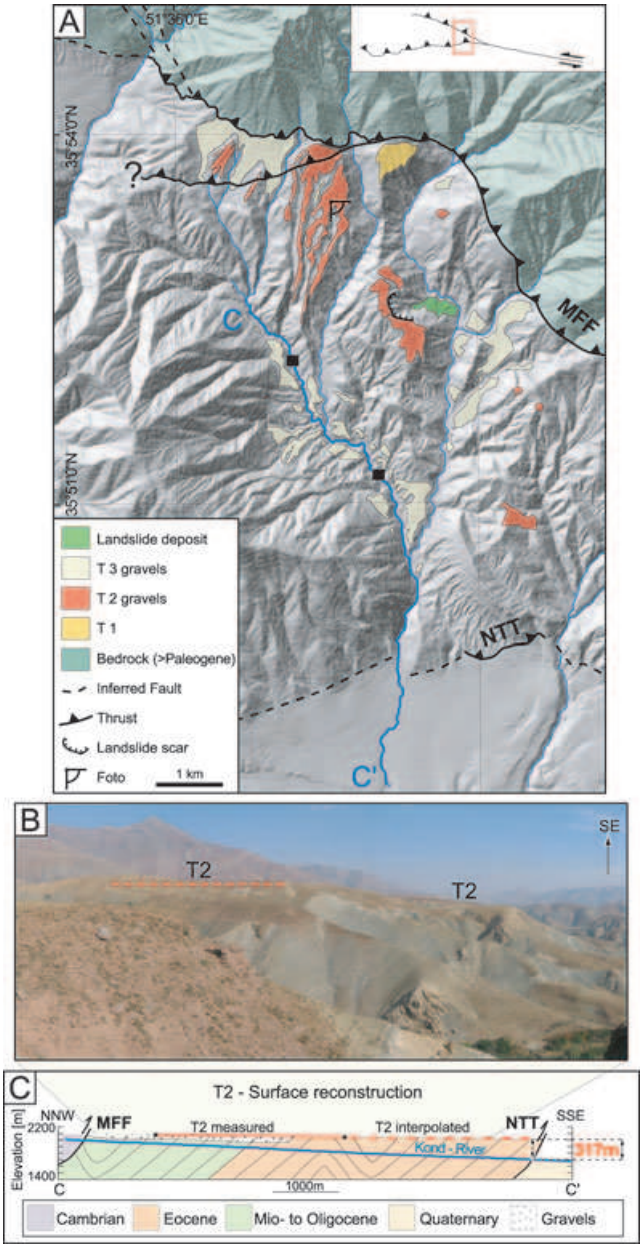

Figure 7. Geological-geomorphic map of the Kond-Valley in the NTT hanging wall and MFF footwall. (a) Three terrace systems occur in the NTT hanging wall (T1-T3), indicating repeated Quaternary uplift along this NTT segment. The MFF is characterized by a step in topography. However, streams cross the MFF without deflection or offset. Recent faulting is manifested with a scarp at a young dip-slip splay fault of MFF. Inset: Figure location with respect to the MFF–NTT system. (b) Terrace T2, a very extensive, gravel-covered palaeopediment, sculpted into folded and tilted Eocene to Miocene units. (c) Two terrace profiles, developed in dip-direction (the upper one from Differential-GPS measurements, the lower one from DEM) were extrapolated by linear best fit to their location above the recent Kond river (black dots in (a) and (c). These points in turn were extrapolated towards the NTT location. The reconstruction of terrace T2 revealed an uplift of 317 m relative to the erosion base at NTT location.

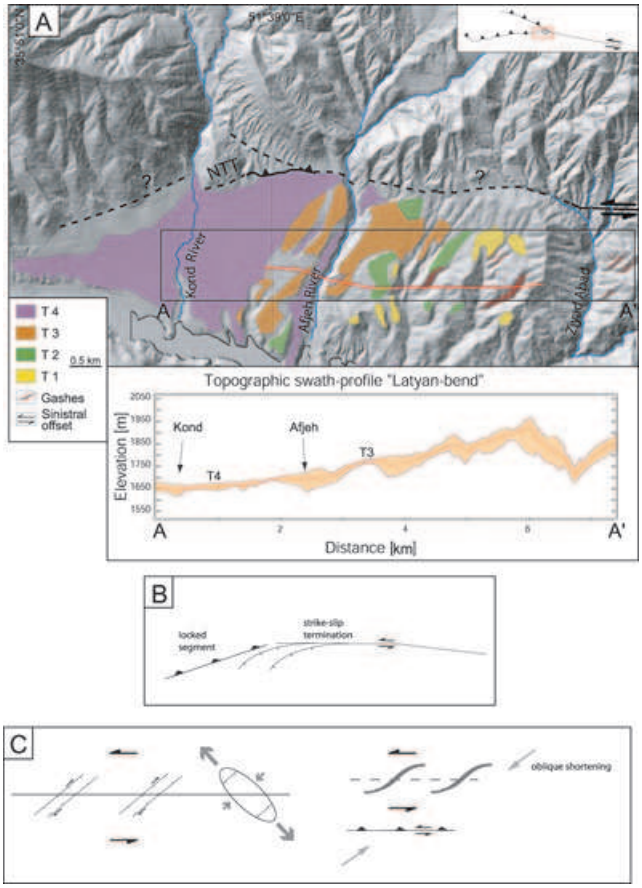

Figure 8. Eastern segment of NTT with footwall deformation: Left-lateral stream offsets are observed at the eastern termination of NTT (right middle in panel a), whereas the western prolongation is characterized by thrust-movement (compare Fig. 7). West of Kond the NTT fault trace is covered by recent sediment. Alternatively, the sinuosity of the mountain front may also rather indicate thrusting and widening of valley by lateral erosion. The footwall topography decreases [(a) and swath-inset], and the terraces become increasingly abandoned westward, indicating a pull-apart basin. This may result from the left bending of the fault or a horsetail-termination related strike-slip motion (b). Note S-shaped closed valleys, aligned along an E–W striking, vertical splay fault (middle of figure, compare Figs 4e–g), interpreted as en échelon aligned macroscale extensional gashes. The extensional direction, inferred from the tension gashes matches the neotectonic stress field (c – sketch after Burbank & Anderson (2001), where extension fractures are formed in response to a strike-slip shear couple), their sigmoidal shapes suggest sinistral shearing (d – sketch after Philip & Meghraoui (1983), with the creation of oblique grabens in response to shortening, which is oblique to the thrust front). Inset in (a): Figure location with respect to the MFF–NTT.

tectono-geomorphic features, including four generations of abandoned surfaces (T1–T4). These terraces occur at increasingly lower elevations towards the west, which is in agreement with the decreasing degree of incision of the surfaces.

An E–W striking, almost vertical splay fault (Latyan Fault, compare Fig. 4g) offsets sediments of Plio-Pleistocene age (Unit A). The fault activity is postdated by terrace T4. This structure was originally a dip-slip fault with up to the south motion, as inferred from rotated clasts in the fault zone, a missing palaeosol (Figs 4g, e and f, respectively), and the deep incision of streams south of it (Fig. 8a). However, horizontal striations developed in a fault gouge also indicate strike-slip reactivation, and the en échelon alignment of map-scale extensional gashes that form sigmoidally shaped depressions (Figs 8a and d) point towards sinistral shear. The extension direction inferred from these gashes is ENE–WSW, matching the present-day tectonic stress field.

6 DISCUSSION AND CONCLUSIONS

Applying Anderson's theory of faulting (Anderson 1905; Anderson 1951), our fault kinematic study revealed an early dextral kinematic history for the NTT and the central MFF. In a few cases the dextral kinematic indicators clearly postdate earlier dip-slip reverse faulting. Miocene dextral strike-slip and oblique reverse faulting along the MFF and NTT took place during NW-oriented shortening. The dextral kinematics are compatible with observations by Axen *et al.* (2001). Zanchi *et al.* (2006) documented dextral transpression during NW-shortening. Partly refolded NE-trending fold axes in the hanging wall of the NTT observed by Allen *et al.* (2003), support such a scenario. Hence, it is reasonable to infer that the E–W striking NTT is mechanically linked with the dextral transpressional alignment along the MFF (Fig. 2). However, the regional expression of this alignment is incompatible with the domal structure used in an early study by Allen *et al.* (2003) to estimate the maximum MFF offset. When restored, this structure would cross the MFF, instead being part of a former alignment. The high-uplift zone between the subvertical western segments of the MFF and Taleghan fault, as observed from topographic residuals, also fits the alignment. The elongated area therefore might be related to uplift under the dextral transpressional regime (Table 1).

Conversely, Allen *et al.* (2003) and Guest *et al.* (2006a) interpreted strike-slip faulting in this region with conjugate dextral and sinistral strike-slip movements during N–S shortening. The early dextral strike-slip regime was superseded by Pliocene NE-oriented shortening, which was associated with sinistral-oblique thrusting along the NTT and the central-western MFF, sinistral strike-slip motion on subsidiary faults in the central MFF segment, and folding and tilting of Eocene to Miocene units in the MFF footwall (Table 1). This is compatible with observations in other areas of the central Alborz mountains (e.g. Axen *et al.* 2001; Allen *et al.* 2003; Guest *et al.* 2006a; Zanchi *et al.* 2006; Moinabadi & Yassaghi 2007). The formation of gravel covered erosion surfaces in these tilted units was accompanied by continued thrusting along the NTT. However, folding in the hanging wall and sinistral stream-offsets indicate a left-oblique component or a Quaternary strike-slip reactivation of the eastern NTT-segment, close to its termination (Table 1). Here, the NTT has an approximate E–W strike, similar to the active, eastern sinistral MFF segment. It is therefore possible that the NTT is favourably oriented to accommodate overall shortening by sinistral strike-slip movement. In addition, the high residual relief in the inside corner of a NTT–EDF system and the topographic along-strike profiles of the NTT suggest that these segments have been not only active, but also very efficient in uplifting this block of the mountain front. An accommodation of left-lateral motion at the eastern NTT is also compatible with the sigmoidal-shaped en échelon tension gashes in the vicinity of the reactivated Latyan fault (Fig. 8). Farther west, the left-bending section of the NTT changes into a dip-slip fault, as indicated by uplifted fluvial terraces and a much more sinuous mountain front. In such a scenario the area west of the Afjeh river would constitute a horsetail termination of a sinistral strike-slip system, causing the opening of a small basin with successive lowering of the local base level of the NTT footwall towards the west (compare Figs 8a–c).

The macroscale pattern of the MFF and the NTT, as part of a former dextral transpressional system, and the present-day sinistral regime observed at the eastern and central-eastern MFF and along the eastern NTT suggest mechanical linkage, and therefore kinematic interaction of both fault systems. Our observations allow for three possible scenarios of fault interaction of this area (Fig. 9).

First, the MFF–NTT system could represent a master fault resulting from eastward propagation of the NTT, which may have eventually reached the MFF (Fig. 9a). This linkage created a longer master fault that increasingly accommodated more displacement. At present, such a structure would take up all of the strain in the deforming area. In contrast, the previously important western and central-western MFF branches would therefore correspond to a stress shadow and would have become inactive. Analogous progressive linkage processes have been recorded by field observations elsewhere (Gupta *et al.* 1998) and by numerical modeling (Cowie *et al.* 1993).

Table 1. Synopsis of simple and composite landscape and structural compartments in the south-central Alborz.

Feature	NW-compression	NE-compression	General description of the observed structure
Topography	High uplifted sectors between the western segments of MFF and Taleghan-Fault	High uplift zone at the inside corner of NTT-EDF	Topographic residuals as indicators of high-incision/high-uplift zones (compare Fig. 6B)
Macroscale structures	NE-trending folds, NE-striking thrusts, MFF-alignment	NW-trending folds, NW-striking thrusts, NE-tilted units	Two sets of large-scale folds (Fig. 2); refolded folds
Mesoscale structures	Conjugate low-angle NE- and WNW-striking dextral oblique thrusts; NE-striking thrusts; high-angle NW-striking left-lateral strike-slip faults; NNE-striking reverse faults, and NE-trending folds	Oblique thrusting along the central MFF and in its footwall, as well as sinistral strike-slip faulting on minor faults in the central MFF segment; NW-striking reverse and thrust faults, and NNE-striking dextral strike-slip faults	Fold axes, directly measured in the field or calculated from measurements of the limbs; compare inset in Figs 5a and b); measured fault-kinematic data based on striations and slickensides, compare Fig. 5)
Quaternary offsets	No obvious signal	Offset terraces in NTT hanging wall, offset streams at easternmost NTT	Gravel covered erosion surface, sculpted into folded Eocene to Miocene units; channels at the NTT are offset or deflected left-laterally; compare Figs 7 and 8

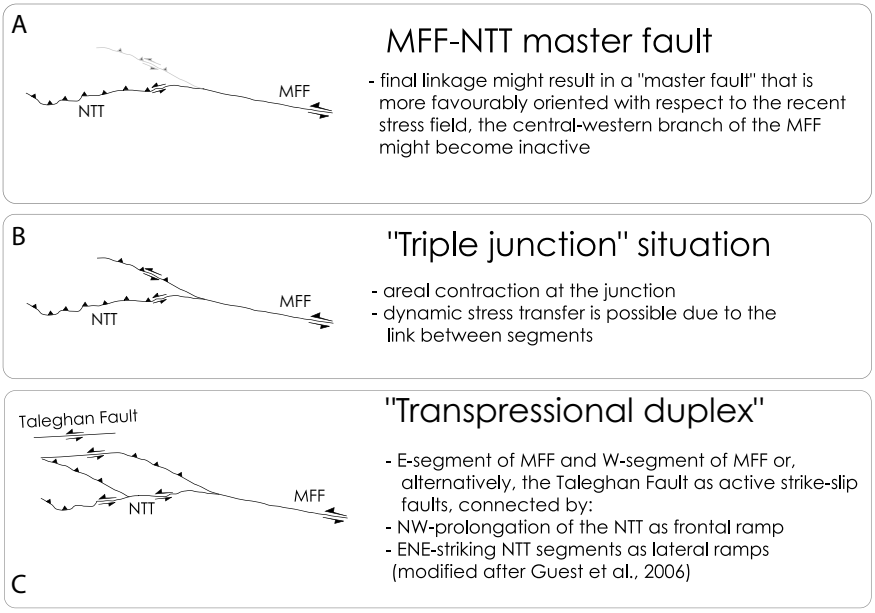

Figure 9. Three possible scenarios depicting fault interaction of this area: (a) The NTT-eastern MFF system could represent a master-fault, (b) The connection of the faults is comparable to a triple junction and (c) the faults are part of a transpressional duplex.

In a second possible scenario, the active fault systems correspond to a situation comparable to a triple junction (Fig. 9b). Here, fault interaction and stress transfer would result in shortening or extension in adjacent areas. Dynamic stress transfer is possible due to the link between segments.

In the third alternative, the MFF and NTT form an integral part of a transpressional duplex (Fig. 9c). In this case, which is modified from the model of Guest *et al.* (2006a), the eastern and western segments of the MFF correspond to active strike-slip faults, connected by a NW prolongation of the NTT as frontal ramp, and ENE-striking NTT segments that form lateral ramps. This model could reconcile the different kinematic styles along the MFF. Accordingly, the dominant kinematics of the NTT segments must be left-lateral motion.

6.1 Master-fault scenario

The most obvious arguments for a master-fault scenario are the missing geomorphic indicators for Holocene faulting along the central-western segment of the MFF, whereas such indicators exist for the adjacent NTT. Moreover, the observed left-lateral kinematics of the easternmost NTT strand follows a similar motion of the MFF, and the affected NTT branch has approximately the same strike as the eastern MFF. It is therefore reasonable to assume that the NTT is more favourably orientated to accommodate sinistral shearing under the present-day stress field than the NW-bending MFF branch. In addition, the NTT–EDF bounded area of high-uplift signals more important block movement there than along the central MFF. However, several observations are incompatible with an inactive MFF branch. First, even if the main present-day seismic activity is observed at the eastern MFF branch, individual small events are also recorded at the central MFF and between the western Taleghan and MFF segments (Ashtari *et al.* 2005). Second, the historical earthquakes have affected different segments of the MFF as a whole. Especially the destructive earthquake from 958AD was probably associated with ruptures of the western MFF segment (Tchalenko 1974; Ambraseys & Melville 1982; Berberian 1983; Berberian & Yeats 2001). These destructive earthquakes did not leave a significant geomorphic mark, as it would be expected for repeated historical ruptures. Nevertheless, the pronounced break in the topography and moreover the palaeo-pediment in the Kond-Valley (compare Fig. 7) imply that the mountain front, which is bounded by the central-western MFF, has been active during Quaternary time.

6.2 Triple-junction scenario

The triple-junction scenario, in its simplest form the intercept of the NTT, the eastern MFF, and the central-western MFF, would allow for coeval deformation along both, the NTT and the MFF. It also could account for the different kinematics of the MFF at the NW-bend. The triple junction concept, originally developed to test whether the geometric constellation, in which three plates meet, is stable or not (e.g. McKenzie & Morgan 1969), was also used to analyse fault junctions (e.g. Peltzer & Tapponnier 1988; Spotila & Anderson 2004; Raterman *et al.* 2007). Since a slip-rate is to date only available for the eastern MFF segment, the fault-junction analysis is limited to the geometric aspect. Overall, the geometry of the MFF–NTT junction is in a stable condition. However, simple motion diagrams of the fault system cannot fully account for the observed late Neogene to Quaternary kinematics (Fig. 10). Assuming three rigid blocks between the faults, we have first inferred the central-western MFF as thrust, the NTT as left-oblique thrust, and solved for the eastern MFF to compare the diagram with the long-term deformation signal, which we suggest to be coherent with the geomorphic signature. The resultant vector for the eastern MFF segment is longest, but would correspond to thrusting with only a minor component of sinistral motion. To increase the strike-slip fraction here, while the geometries of the other fault segments are kept, the shortening at the central-western MFF segment has to become significantly smaller. Therefore, with the observed kinematics coeval activity of all three faults is difficult to reconcile. However, the diagram suggests the highest slip rates occur at the eastern MFF segment. Slip would become distributed over the branching faults, which is a reasonable assumption for the studied area.

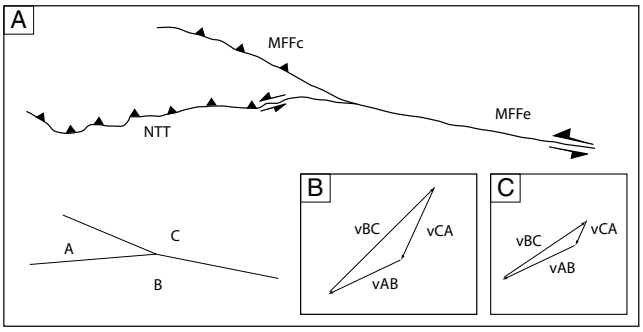

Figure 10. Simple motion diagram to explain the MFF–MFF–NTT fault junction. (a) Simplified fault segment geometry as observed in the field with indication of thrusting along the central MFF segment, and left-oblique thrusting at the NTT. (b) The simple motion diagram shows that the resultant vector for the eastern MFF is the longest. This means that this segment would experience the highest rate, coherent to what is observed in the present-day seismicity. However, the direction of motion indicates a primary thrusting with only a minor component of sinistral motion. To increase the strike-slip component here, the shortening at the central-western MFF segment has to become significantly smaller (c).

6.3 Transpressional duplex scenario

Under the present-day stress field, a transpressional duplex would transfer the left-lateral to oblique-reverse motion along the MFF in order to accommodate shortening in this part of the mountain range. The model therefore accounts for the observed sinistral motion along the eastern MFF branch and the kinematic change towards thrusting or left-oblique thrusting in the central and western segments, respectively. Within such a duplex structure, the elevated topography north of Tehran would be created by westward thrusting along the NW-striking central MFF-segment and similar striking, parallel thrusts in the footwall. Active frontal ramps in this system are the EDF, the PVT and the NW prolongation of the NTT. The EDF is, together with the NTT, responsible for the high residual relief of the Touchal block. The fact that the NW-striking PVT and EDF are observed only in the hanging wall of the NTT and do not cut the fault, suggests either kinematic linkage of these faults with the NTT or that the NTT movement postdates any activity along the PVT and EDF. However, the northwestern prolongation of the NTT is characterized by a very sinuous range front, indicative of strong lateral erosion into the hanging wall, and therefore low degree of tectonic activity (e.g. Bull 2007).

The NTT and the western MFF do not constitute sinistral tear faults to connect the frontal ramps, even if the present-day stress field would allow for dominant left-lateral kinematics. Instead, the kinematic regime along the NTT is characterized by oblique thrusting or reverse faulting. The fault dip is rather steep and the wide fault zone in the hanging wall strikes parallel to the NTT and rather documents S-, than W-directed movement. The NTT-segments therefore may represent lateral ramps and the steep fault dip might eventually flatten with depth. The along-strike topographic profiles of the NTT also reveal a semi-independent deformation history, which might be coupled with deformation along the NW-striking thrusts in the hanging wall. However, the central NTT segment, which accommodated the highest amount of deformation, starts already in the footwall of the EDF (Fig. 6).

Taken together, our data show that a transpressional duplex system was not the first-order structure at the onset of the evolution of this part of the mountain range. Instead, the duplex is a young structure, probably associated with the changeover from regional NW- to NE-shortening. The inherited topography and uplift history might be responsible for this modification. The en échelon array of the NTT might have favoured the development of thrust sheets under the recent stress field. This scenario is in agreement with the fact that such a clear linkage with the NW-striking faults is not observable for the western MFF segment, which suggests that these faults, starting from the NTT, might propagate northwestward. The transpressional duplex therefore is in a nascent stage. The distribution of the residual relief, which often corresponds to areas of highest uplift (e.g. Bürgmann *et al.* 1994), suggests that the Touchal block, which is thrust along the EDF and bounded by the central and eastern NTT-segments, as well as the central-western MFF, was uplifted most effectively. In this context, the sinistral changeover at the easternmost NTT is indicative of a jump of the deformation front onto this block.

In conclusion, our data suggest an early mechanical linkage of the NTT and MFF fault systems during a former dextral transpressional stage under NW-shortening. This regime, however, was superseded by Pliocene to Recent NE-oriented shortening. Resulting from this reorganization, the NTT and MFF were reactivated and incorporated into a nascent transpressional duplex. This system has prevailed for a significant duration of deformation. However, the youngest period is characterized by an extensional regime, which might invert the observed structure. Importantly, this system has not yet erased the topographic signal of the transpressional arrangement.

ACKNOWLEDGMENTS

This work was funded by the German Research Council (DFG project STR 373/19 − 1 and funds from the DFG Leibnitz Award to M. Strecker). We greatly appreciate logistical help from the Tehran Building and Housing Research Center. In particular, we would like to thank A.H. Heidarinejad, T. Parhizkar and A.H. Mirzaei for their encouragement. We wish to thank Y. Djamour, M. Shakeri and M. Hekmatnia for their logistical GPS support, and B. Fabian for her help with the illustrations. Our interpretations have benefited from discussions with J. Jackson, J.-F. Ritz and J.R. Arrowsmith. Special thank to Prof. G. Hilley and an anonymous reviewer as well as the editor Dr Y. Ben-Zion for very helpful and constructive comments.

REFERENCES

Alavi, M., 1991. Sedimentary and structural characteristics of the Paleo-Tethys remnants in northeastern Iran, *Geol. Soc. Am. Bull.,* **103,** 983–992.

Alavi, M., 1996. Tectonostratigraphic synthesis and structural style of the Alborz Mountain system in northern Iran, *J. Geodyn.,* **21,** 1–33.

Allen, M.B., Ghassemi, M.R., Shahrabi, M. & Qorashi, M., 2003. Accomodation of late Cenozoic oblique shortening in the Alborz range, northern Iran, *J. Struct. Geol.,* **25,** 659–672.

Allenbach, P., 1966. Geologie and Petrographie des Demavand und seiner Umgebung (Zentral-Elburz, Iran), *Mitteilungen aus dem Geologischen Institut der Eidgenö ssischen Technischen Hochschule und der Universität Zürich*, 1–144.

Allmendinger, R., 2001. FaultKinWin, http://www.geo.cornell.edu/geology/faculty/RWA/programs.html.

Ambraseys, N.N., 1974. Historical seismicity of north-central Iran, *Material for the Study of Seismotectonics of Iran: North-central Iran,* Geological Survey of Iran, Report, **29,** 47–96.

Ambraseys, N.N. & Melville, C.P., 1982. *A History of Persian Earthquakes*, Cambridge University Press, London, 219 pp.

Anderson, E.M., 1905. The dynamics of faulting, *Trans. Edinburgh Geol. Soc.,* **8,** 387–402.

Anderson, E.M., 1951. *The Dynamics of Faulting and Dyke Formation with Applications to Britain*, 2nd edn, Oliver and Boyd, Edinburgh.

Anderson, G. & Ji, C., 2003. Static stress transfer during the 2002 Nenana Mountain-Denali Fault, Alaska, earthquake sequence, *Geophys. Res. Lett.,* **30,** 1310–1315.

Anderson, G., Aagaard, B. & Hudnut, K., 2003. Fault interactions and large complex earthquakes in the Los Angeles area, *Science,* **302,** 1946–1949.

Armijo, R., Meyer, B., King, G.C.P., Rigo, A. & Papanastassiou, D., 1996. Quaternary evolution of the Corinth Rift and its implication for the late Cenozoic evolution of the Aegean, *Geophys. J. Int.,* **126**(1), 11–53.

Armijo, R., Flerit, F., King, G.C.P. & Meyer, B., 2003. Linear elastic fracture mechanics explains the past and present evolution of the Aegean, *Earth planet. Sci. Lett.,* **217,** 85–95.

Arrowsmith, R. & Strecker, M., 1999. Seismotectonic range front segmentation and mountain belt growth along the northern Pamir Mountains, Kyrgyzstan (India-Eurasia collision zone), *Geol. Soc. Am. Bull.,* **111,** 1665–1683.

Ashtari, M., Hatzfeld, D. & Kamalian, N., 2005. Microseismicity in the region of Tehran, *Tectonophysics,* **395,** 193–208.

Assereto, R., 1966. Explanatory notes on the geological map of Upper Djadjerud and Lar Valleys (Central Elburz, Iran), scale 1:50.000. University of Milan (Italy) Institute of Geology, 86 pp.

Axen, G.J., Lam, P.S., Grove, M. & Stockli, D.F., 2001. Exhumation of the west-central Alborz mountains, Iran, Caspian subsidence, and collision-related tectonics, *Geology,* **29**(6), 559–562.

Aydin, A. & Schultz, R.A., 1990. Effect of mechanical interaction on the development of strike-slip faults with echelon patterns, *J. Struct. Geol.,* **12**(1), 123–129.

Bachmanov, D.M. *et al.*, 2004. Active faults in the Zagros and central Iran, *Tectonophysics,* **380,** 221–241.

Ballato, P., Nowaczyk, N., Landgraf, A., Strecker, M.R., Friedrich, A. & Tabatabaei, S.H., 2008: tectonic control on sedimentary facies pattern and sediment accumulation rates in the Miocene foreland basin of the southern Alborz mountains, northern Iran, *Tectonics,* **27,** TC6001.

Barka, A. *et al.*, 2002. The Surface Rupture and Slip Distribution of the 17 August 1999 Izmit Earthquake (M 7.4), North Anatolian Fault, *Bull. seism. Soc. Am.,* **92**(1), 43–60.

Bennett, R., Furlong, K. & Friedrich, A., 2004. Codependent histories of the San Andreas and San Jacinto fault zones from inversion of fault displacement rate, *Geology,* **32**(11), 961–964.

Berberian, M., 1983. Continental deformation in the Iranian Plateau, Contribution of Seismotectonics of Iran, Geological Survey of Iran, Report 52, 625 pp.

Berberian, M. & Yeats, R.S., 1999. Patterns of historical earthquake rupture in the Iranian Plateau, *Bull. seism. Soc. Am.,* **89,** 120–139.

Berberian, M. & Yeats, R.S., 2001. Contribution of archeaological data to studies of earthquake history in the Iranian Plateau, *J. Struct. Geol.,* **23,** 563–584.

Bilham, R. & King, G., 1989. The morphology of strike-slip faults: examples from the San Andreas Fault, California, *J. geophys. Res.,* **94**(B8), 10 204–10 216.

Brankman, C.M. & Aydin, A., 2004. Uplift and contractional deformation along a segmented strike-slip fault system: the Gragano Promontory, southern Italy, *J. Struct. Geol.,* **26,** 807–824.

Bürgmann, R., Arrowsmith, R. & Dumitru, T., 1994. Rise and fall of the southern Santa Cruz Mountains, California, from fission tracks, geomorphology, and geodesy, *J. geophys. Res.,* **99**(B10), 20 181–20 202.

Bull, W., 2007. *Tectonic Geomorphology of Mountains. A New Approach to Paleoseismology*, Blackwell Publishing, Oxford.

Burbank, D.W. & Anderson, R.S., 2001. *Tectonic Geomorphology*, Blackwell Science, Oxford.

Burbank, D.W., Meigs, A. & Brozovic, N., 1996. Interactions of growing folds and coeval depositional systems, *Basin Res.,* **8,** 199–223.

Burbank, D.W., McLean, J.K., Bullen, M., Abdrakhmatov, K.Y. & Miller, M.M., 1999. Partitioning of intermontane basins by thrust-related folding, Tien Shan, Kyrgystan, *Basin Res.,* **11,** 75–92.

Célérier, B., 1995. Tectonic regime and slip orientation of reactivated faults, *Geophys. J. Int.,* **121,** 143–161.

Cowie, P.A., Vanneste, C. & Srnette, D., 1993. Statistical physical model for the spatio-temporal evolution of faults, *J. geophys. Res.,* **98,** 21 809–21 821.

Cowie, P.A., Gupta, S. & Dawers, N.H., 2000. Implications of fault array evolution for syn-rift depocentre development: insights from a numerical fault growth model, *Basin Res.,* **12,** 241–261.

Dawers, N.H., Anders, M. & Scholz, Ch.H., 1993. Growth of normal faults: displacement-length scaling, *Geology,* **21,** 1107–1110.

Davoudzadeh, M. & Schmidt, K., 1984. A review of the Mesozoic paleogeography and paleotectonic evolution of Iran, *Neues Jahrbuch für Geologie und Paläontologie, Abhandlungen,* **168**(2/3), 182–207.

Dellenbach, J., 1964. Contribution a I' etude geologique de region situess al' est de Tehran (Iran), *PhD dissertation*, Fac. Sci., Univ. Strasbourg, France, 117 p.

De Martini, P.M., Hessami, K., Pantosi, D., Addezio, G.D., Alinaghi, H. & Ghafory-Ashtiani, M., 1998. A geologic contribution to the evaluation of the seismic potential of the Kahrizak fault (Tehran, Iran), *Tectonophysics,* **287,** 187–199.

Densmore, A.L., Dawers, N.H., Gupta, S., Allen, P.A. & Gilpin, R, 2003. Fault growth and landscape evolution at extensional relay zones. *J. geophys. Res.,* **108**(B5), 2273.

Densmore, A.L., Gupta, S., Allen, P.A. & Dawers, N.H., 2003. Transient landscapes at fault tips, *J. geophys. Res.,* **112,** F03S08.

Dolan, J.F., Bowman, D.D. & Sammis, C.G., 2007. Long-range and long-term fault interactions in Southern California, *Geology,* **35**(9), 855–858.

Eberhart-Phillips, D. *et al.*, 2003. The 2002 Denali Fault Earthquake, Alaska: a large magnitude, slip-partitioned event, *Science,* **300,** 1113–1118.

Engalenc, M., 1968. Contribution a la Geologie, Geomorphologie, Hydrogeologie de la region de Tehran (Iran), *C.E.R.H., Montpellier, France*, 365 p.

Fakhari, M.D., Axen, G.J., Horton, B.K., Hassanzadeh, J. & Amini, A., 2008. Revised age of proximal deposits in the Zagros foreland basin and implications for Cenozoic evolution of the High Zagros, *Tectonophysics,* **451,** 170–185.

Friedrich, A.M., Wernicke, B., Niemi, N.A., Bennett, R.A. & Davis, J.L., 2003. Comparison of geodetic and geologic data from the Wasatch region, Utah, and implications for the spectral character of Earth deformation at periods of 10 to 10 million years, *J. geophys. Res.,* **108**(B4), 2199.

Guest, B., Axen, G.J., Lam, P.S. & Hassanzadeh, J., 2006a. Late Cenozoic shortening in the west-central Alborz Mountains, northern Iran, by combined conjugate strike-slip and thin-skinned deformation, *Geosphere,* **2,** 35–52.

Guest, B., Stockli, D.F., Grove, M., Axen, G.J., Lam, P.S. & Hassanzadeh, J., 2006b. Thermal histories from the central Alborz mountains, northern Iran: implications for the spatial and temporal distribution of deformation in northern Iran, *Geol. Soc. Am. Bull.,* **118**(11/12), 1507–1521.

Gupta, S., Cowie, P.A., Dawers, N.H. & Underhill, J.R., 1998. A mechanism to explain rift-basin subsidence and stratigraphic patterns through fault-array evolution, *Geology,* **26**(7), 595–598.

Hartleb, R.D. *et al.*, 2002. Surface Rupture and Slip Distribution along the Karadere Segment of the 17 August 1999 Izmit and the Western Section of the 12 November 1999 Düzce, Turkey, Earthquakes, *Bull. seism. Soc. Am.,* **92**(1), 67–78.

Hilley, G.E., Arrowsmith, J.R. & Buergman, R., 1997. Investigation of Active Deformation Using a Landscape Development Model and Field Examination of Landforms and Geology along the Northeastern Margin of the Southern Santa Cruz Mountains, Geological Society of America Abstracts with Programs, 1997 Annual Meeting.

Hubert-Ferrari, A., Barka, A., Jaques, E., Nalbant, S., Meyer, B., Armijo, R., Tapponier, P. & King, G.C.P., 2000. Seismic hazard in the Marmara Sea region following the 17 August 1999 Izmit earthquake, *Nature,* **404,** 269–273.

Jackson, J., Norris, R. & Youngson, J., 1996. The structural evolution of fault and fold systems in central Otago, New Zealand: evidence revealed by drainage patterns, *J. Struct. Geol.,* **18,** 217–234.

Jackson, J.A., Priestley, K., Allen, M.B. & Berberian, M., 2002a. Active tectonics of the South Caspian Basin, *Geophys. J. Int.,* **148,** 214–245.

Jackson, J., Ritz, J.F., Siame, L., Raisbeck, G., Yiou, F., Norris, R., Youngson, J. & Bennett, E., 2002b. Fault growth and landscape development rates in Otago, New Zealand, using in situ cosmogenic 10Be, *Earth planet. Sci. Lett.,* **195,** 185–193.

Keller, E.A., Zepeda, R.L., Rockwell, T.K., Ku, T.L. & Dinklage, W.S., 1998. Active tectonics at Wheeler Ridge, southern San Joaquin Valley, California, *Geol. Soc. Am. Bull.,* **110,** 298–310.

Keller, E.A., Gurrola, L. & Tierney, T.E., 1999. Geomorphic criteria to determine direction of lateral propagation of reverse faulting and folding, *Geology,* **27,** 515–518.

King, G.C.P., Stein, R. & Rundle, J.B., 1988. The growth of geological structures by repeated earthquakes 1. Conceptual framework, *J. geophys. Res.,* **93**(11), 13 307–13 318.

King, G., Klinger, Y., Bowman, D. & Tapponnier, P., 2005. Slip-Partitioned Surface Breaks for the Mw 7.8 2001 Kokoxili Earthquake, China, *Bull. seism. Soc. Am.,* **95**(2), 731–738.

Kürsten, M., 1980. Zur geodynamischen Entwicklung des Iran, ein Beispiel intrakratonischer struktureller Vorgänge, *Int. J. Earth Sci.,* **69**(1), 22–40.

Lin, J. & Stein, R., 2004. Stress triggering in thrust and subduction earthquakes and stress interaction between the southern San Andreas and nearby thrust and strike-slip faults, *J. geophys. Res.,* **109,** 975–978.

McKenzie, D.P. & Morgan, W.J., 1969. Evolution of Triple Junctions, *Nature,* **224,** 125–133.

Merrits, D. & Vincent, K.R., 1989. Geomorphic response of coastal streams to low, intermediate, and high rates of uplift, Mendocino triple junction region, Northern California, *Geol. Soc. Am. Bull.,* **101,** 1373–1388.

Meyer, B., Tapponnier, P., Bourjot, L., Metivier, F., Gaudemer, Y., Peltzer, G., Shunmin, G. & Zhitai, C., 1998. Crustal thickening in Gansu-Qinghai, lithospheric mantle subduction, and oblique, strike-slip controlled growth of the Tibet plateau, *Geophys. J. Int.,* **135,** 1–47.

Moinabadi, M.E. & Yassaghi, A., 2007. Geometry and kinematics of the Mosha Fault, south central Alborz Range, Iran: an example of basement involved thrusting, *J. Asian Earth Sci.,* **29**(5-6), 928–938.

Niemi, N.A., Wernicke, B.P., Friedrich, A.M., Simons, M., Bennet, R.A. & Davis, J.L., 2004. BARGEN continuous GPS data across the eastern Basin and Range province, and implications for fault system dynamics, *Geophys. J. Int.,* **159,** 842–862.

Peltzer, G. & Tapponnier, P., 1988. Formation and evolution of strike-slip faults, rifts, and basins during the India-Asia collision: an experimental approach, *J. geophys. Res.,* **93**(12), 15 085–15 117.

Peltzer, G., Crampé, F., Hensley, S. & Rosen, P., 2001. Transient strain accumulation and fault interaction in the Eastern California shear zone, *Geology,* **29**(11), 975–978.

Philip, H. & Meghraoui, M., 1983. Structural analysis and interpretation of the surface deformations of the El Asnam earthquake of October 10, 1980, *Tectonics,* **2,** 17–49.

Pollard, D.D. & Aydin, A., 1988. Progress in understanding jointing over the past century, *Geol. Soc. Am. Bull.,* **100,** 1181–1204.

Pollard, D.D. & Fletcher, R.C., 2005. *Fundamentals of Structural Geology*, Cambridge University Press, Cambridge.

Pollitz, F.F. & Sacks, S.I., 2002. Stress triggering of the1999 Hector Mine eartquakes by transient deformation following the 1992 Landers earthquakes, *Bull. seism. Soc. Am.,* **92**(4), 1487–1496.

Priestley, K., Baker, C. & Jackson, J., 1994. Implications of earthquake focal mechanism data for the active tectonics of the south Caspian Basin and surrounding regions, *Geophys. J. Int.,* **118,** 111–141.

Raterman, N.S., Cowgill, E. & Lin, D., 2007. Variable structural style along the Karakoram fault explained using triple-junction analysis of intersecting faults, *Geosphere,* **3**(2), 71–85.

Rieben, H., 1955. The geology of the Teheran Plain, *Am. J. Sci.,* **253,** 617–639.

Ritz, J.-F., Nazari, H., Ghassemi, A., Salamati, R., Shafei, A., Solaymani, S. & Vernant, P., 2006. Active transtension inside Central Alborz: a new insight into the northern Iran-southern Caspian geodynamics, *Geology,* **34**(6), 477–480.

Rockwell, T.K., Lindvall, S., Herzberg, D., Murbach, D., Dawson, T. & Berger, G., 2000. Paleoseismology of the Johnson Valley, Kickapoo, and Homestead Valley faults: clustering of earthquakes in the eastern California shear zone, *Bull. seism. Soc. Am.,* **90,** 1200–1236.

Sanderson, D.J. & Marchini, W.R.D., 1984. Transpression, *J. Struct. Geol.,* **6**(5), 449–458.

Spotila, J.A. & Anderson, K.B., 2004. Fault interaction at the junction of the Transverse Ranges and Eastern California shear zone: a case study of intersecting faults, *Tectonophysics,* **379,** 43–60.

Stampfli, G.M. & Borel, G.D., 2002. A plate tectonic model for the Paleozoic and Mesozoic constrained by dynamic plate boundaries and restored synthetic oceanic isochrons, *Earth planet. Sci. Lett.,* **196,** 17–33.

Steiger, R., 1966. Die Geologie der west-Firuzkuh-Area (Zentralelburz, Iran), Mitteilungen aus dem geologischen Institut der Eidgenössischen Technischen Hochschule und der Universität Zürich, Neue Serie, 1–145.

Stein, R., King, G.C.P. & Rundle, J.B., 1988. The growth of geological structures by repeated earthquakes 2. Field examples of continental dip-slip faults, *J. geophys. Res.,* **93**(11), 13 319–13 331.

Stein, R.S., Barka, A.A. & Dieterich, J.H., 1997. Progressive failure on the North Anatolian fault since 1939 by earthquake stress triggering, *Geophys. J. Int.,* **128,** 594–604.

Strecker, M., Blisniuk, P. & Eisbacher, G., 1990. Rotation of extension direction in the central Kenya Rift, *Geology,* **18,** 299–302.

Strecker, M.R., Hilley, G., Arrowsmith, J. R. & Coutand, I., 2003. Differential structural and geomorphic mountain-front evolution in an active continental collision zone: the NW Pamir, southern Kyrgyzstan, *Geol. Soc. Am. Bull.,* **115,** 166–181.

Taboada, A., Bousquet, J.C. & Philip, H., 1993. Coseismic elastic models of folds above blind thrusts in the Betic Cordilleras (Spain) and evaluation of seismic hazard, *Tectonophysics,* **220,** 223–241.

Teyssier, C. & Tikoff, B., 1998. Strike-slip partitioned transpression of the San Andreas fault system: a lithospheric-scale approach, in *Continental Transpressional and Transtensional Tectonics,* Vol. 135, pp. 143–158, eds Holdsworth, R.E., Strachan, R.A. & Dewey, J.F., Geological Society, London, Special Publications.

Teyssier, C., Tikoff, B. & Markley, M., 1995. Oblique plate motion and continental tectonics, *Geology,* **23**(5), 447–450.

Tchalenko, J.S., 1974. Tectonic framework of the Tehran region, in *Material for the Study of Seismotectonics of Iran: North-central Iran, Geological Survey of Iran, Report* **29,** 7–46.

Tchalenko, J.S., 1975. Seismotectonic framework of the North Tehran Fault, *Tectonophysics,* **29,** 411–420.

Vernant, P. *et al.*, 2004a. Present-day crustal deformation and plate kinematics in the Middle East constrained by GPS measurements in Iran and northern Oman, *Geophys. J. Int.,* **157,** 381–398.

Vernant, P. *et al.*, 2004b. Deciphering oblique shortening of central Alborz in Iran using geodetic data, *Earth planet. Sci. Lett.,* **223,** 177–185.

Wesnousky, S.G., 2006. Predicting the endpoints of earthquake ruptures, *Nature,* **444,** 358–360.

Zanchi, A., Berra, F., Mattei, M., Ghassemi, M.R. & Sabouri, J., 2006. Inversion tectonics in central Alborz, Iran, *J. Struct. Geology,* **28**(11), 2023–2037.

Zoback, M.D. *et al.*, 1987. New evidence on the State of Stress of the San Andreas Fault System, *Science,* **238,** 1105–1111.